Journal of Materials Chemistry C

Accepted Manuscript

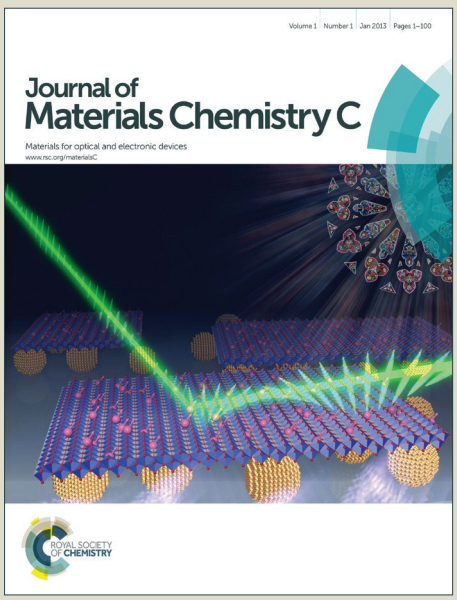

ROYAL SOCIETY OF CHEMISTRY

www.rsc.org/materialsC

Journal of Materials Chemistry C

Journal of Materials Chemistry C

Dynamic Article Links ►

Cite this: DOI: 10.1039/c0xx00000x

ARTICLE TYPE

www.rsc.org/xxxxxx

A Strategy for Enhancing the Sensitivity of Optical Thermometer in β-$NaLuF_4$:Yb^{3+}/Er^{3+} Nanocrystals

Kezhi Zheng, Guanghui He, Weiye Song, Xueqing Bi, and Weiping Qin*

Received (in XXX, XXX) Xth XXXXXXXXX 201X, Accepted Xth XXXXXXXXX 201X
DOI: 10.1039/b000000x

A strategy for enhancing the sensitivity of optical thermometer is developed here by using non-thermal coupled levels of Er^{3+}. Under the excitation of 980 nm laser, the temperature dependence of 244 nm and 256 nm upconversion luminescences (UCLs) of Er^{3+} were studied. The corresponding $^2I_{11/2}$ and $^4D_{7/2}$ levels are confirmed to be non-thermally coupled levels. By using fluorescence intensity ratio (FIR) technique and investigating different thermal population behaviors of $^2I_{11/2}$ and $^4D_{7/2}$ levels, optical temperature sensing performance based on non-thermal coupled levels of Er^{3+} was fulfilled here for the first time. The obtained maximum sensor sensitivity is 0.106 K^{-1} at 525 K, much higher than those of all other RE^{3+} doped optical thermometer using thermal coupled levels-based FIR technique. This suggests that the use of FIR from neighboring non-thermal coupled levels of RE^{3+} is a promising approach for enhancing the sensor sensitivity of optical thermometers.

Introduction

High accuracy and high resolution temperature measurement is a challenging research topic in both scientific and industrial fields.[1–4] Because of the noninvasive mode and quick response, luminescence-based measurement is one of the most important technologies for determining temperature,.[5–8] Recently, non-contact optical temperature sensors based on the fluorescence intensity ratio (FIR) among different emission lines have attracted much interest due to their excellent sensitivity and accuracy.[9–18] Moreover, compared with other temperature measurement techniques, this optical thermometry method can reduce the dependence of testing condition, such as fluorescence loss and electromagnetic compatibility problem, resulting in its potential applications in biocompatible temperature probe, electrical power stations, coal mines, and oil refineries, *etc.*[19–22]

Rare earth ions (RE^{3+}) have multiple energy level structures, the interest in RE^{3+} doped upconversion luminescent (UCL) nanoparticles has experienced a surge within the scientific community owing to the near-infrared (NIR) excitation source and their unique optical characteristics arising from their intra 4*f* transitions.[23–38] In addition, by investigating the energy level distributions of RE^{3+} ions, we find Er^{3+}, Tm^{3+}, Ho^{3+}, Gd^{3+}, Pr^{3+}, and Nd^{3+}, *etc*, have pairs of thermally coupled levels, made them potentially candidates for optical thermometry by using FIR technique. As one of the most important RE^{3+}, Er^{3+} has abundant and ladder-like energy level structure, which is an ideal activator for UCL. More importantly, over the past few years, Er^{3+} doped UCL materials have been widely considered as optical temperature sensor by comparing the emission intensities from thermally coupled electronic levels of $^2H_{11/2}$ and $^4S_{3/2}$.[39–41] As we know, Er^{3+} ions have multiple energy level structures in ultraviolet (UV) region. The UV UCLs of Er^{3+} under the excitation of NIR laser have been reported in fluoride nano/microparticles in our previous works.[42, 43] However, heretofore few results on optical thermometry have been reported mainly concerning the UCLs of Er^{3+} in the UV region.[44, 45]

Generally, the FIR method is implemented by exploiting the temperature-dependent luminescence intensities from two nearby electronic energy levels which are governed by Boltzmann-type population distribution. It is known that the fluorescence intensities are proportional to the population of two thermally equilibrious levels, thus, the FIR can be expressed by $C\exp(-\Delta E/kT)$, where C is a constant, ΔE, k, and T represent the energy difference between the two nearby levels, the Boltzmann constant, and the absolute temperature, respectively. According to the principle of a FIR-based optical thermometer, the sensor sensitivity, which is an important parameter to determine the performance of temperature sensor, is proportional to the energy gap of the corresponding thermally coupled energy levels. As we all know, the larger energy gap is the higher sensor sensitivity is. However, to ensure the upper level of optical activators (RE^{3+}) is thermally populated from their lower levels, the energy difference between the emitting levels of RE^{3+} ions is upper bounded at

about 2000 cm^{-1}. Although the highest sensitivity has reached ~2.8×10^{-2} K^{-1} in $NaYF_4:Nd^{3+}$ microcrystals by using thermal coupled levels of Nd^{3+},[46] further enhancement of the sensing sensitivity is difficult to implement owing to the restriction of energy gap between thermal coupled levels, as mentioned above.

Herein, we presented a strategy for enhancing the sensitivity of temperature sensor by virtue of the non-thermally coupled levels of Er^{3+}. Hexagonal phase (β-) $NaLuF_4$ was chosen as the matrix material in this work. Upon excitation with 980 nm NIR laser, UC emissions of Er^{3+} in the UV region of 235 – 270 nm were investigated. The luminescence intensity ratios of 244 nm to 256 nm of Er^{3+} were discussed systematically by changing the sample temperature. The related thermal behaviors originating from the $^2I_{11/2}$ and $^4D_{7/2}$ states of Er^{3+} were investigated in the temperature range of 300 – 525 K. A high sensitivity was achieved in this UV-based sensor by using non-thermally coupled levels ($^2I_{11/2}$ and $^4D_{7/2}$) of Er^{3+}. The highest sensor sensitivity reached 0.106 K^{-1} in this work, which is prior to all previously reported RE^{3+} doped temperature sensor by exploiting the thermal coupled levels-based FIR technique. This novel temperature sensing performance based on the non-thermally coupled levels of Er^{3+}, combined with their imaging characteristics, made Er^{3+}-based UV UCL materials promising platforms for potential biological applications.

Experimental procedures

Chemicals

The raw chemicals, including $LuCl_3\cdot6H_2O$, $YbCl_3\cdot6H_2O$, $ErCl_3\cdot6H_2O$ (all with purity > 99.999%, Shanghai Shabo Chemical Technology Co., Ltd. China), NaOH, NH_4F (all with the analytically purity, Beijing Fine Chemical Company, China), 1-Octadecene (ODE, 90%, Alfa Aesar) and oleic acid (OA, 90%, Alfa Aesar) were used without further purification.

Sample Preparation

$NaLuF_4:Yb^{3+}/Er^{3+}$ sample was prepared via a thermal decomposition method, which described briefly as follows.[47] In a typical procedure for the synthesis of $NaLuF_4$:20%Yb^{3+}, 1.5%Er^{3+}, 1 mmol $RECl_3\cdot6H_2O$ (RE = Lu, Yb, Er) were added to a 100 mL three-neck round-bottom flask containing a certain amount of ODE and OA. The solution was magnetically stirred and heated to 150 °C for 30 min to remove residual water and oxygen. Then, the temperature was cooled down to room temperature with a gentle flow of argon gas through the reaction flask. Meanwhile, a solution of NH_4F and NaOH dissolved in methanol was added, and then the temperature was increased to 50 °C. After methanol was evaporated, the reaction mixture was heated to 300 °C in an argon atmosphere, kept for 60 min and then naturally cooled to room temperature. The resultant products were precipitated by the addition of ethanol, collected by centrifugation and washed with ethanol three times.

Characterizations

The crystal structure were analyzed by a Rigaku RU-200b X-ray powder diffractometer (XRD) using a nickel-filtered Cu-Kα radiation (λ = 1.5406 Å). The size and morphology of the sample were investigated by transmission electron microscopy (TEM, Hitachi H-600). The UCL spectra were recorded using a Hitachi F-4500 fluorescence spectrophotometer which equipped with a power-controllable 980 nm CW diode laser as excitation source. The temperature of the sample was controlled by using a set of home-made equipment.

Results and discussion

Figure 1(a) shows the XRD pattern of the sample. It is clear that the sample was β-$NaLuF_4$, which was in good agreement with the standard values of JCPDS No.27–726. The morphological analysis of the sample with TEM, as depicted in Fig. 1(b), showed that the as-synthesized $NaLuF_4:Yb^{3+}/Er^{3+}$ nanoparticles were approximately spherical with nearly uniform size distribution. The diameters of $NaLuF_4$ nanospheres were about 40 nm on average.

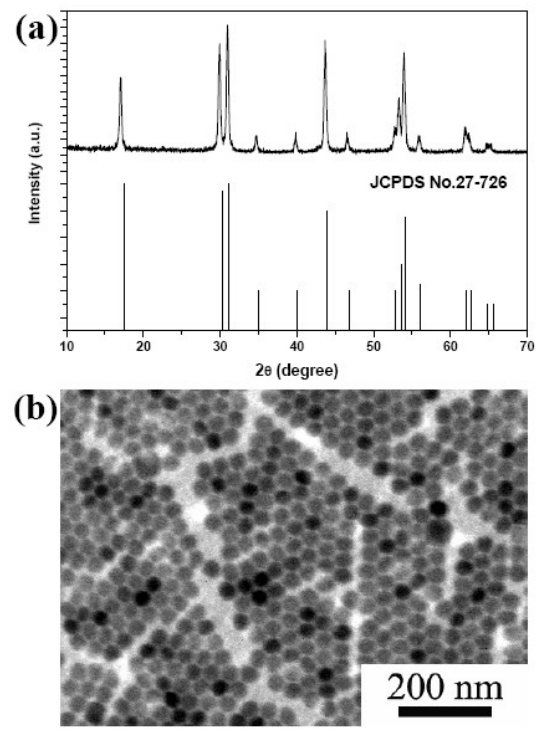

Fig. 1 (a) XRD pattern of $NaLuF_4:Yb^{3+}/Er^{3+}$ nanocrystals and the standard datum for hexagonal phase $NaLuF_4$ (JCPDS No.27-726); (b) TEM image of $NaLuF_4:Yb^{3+}/Er^{3+}$ nanocrystals.

At 980 nm excitation of ~300 mW, the $NaLuF_4:Yb^{3+}/Er^{3+}$ nanocrystals emitted UC luminescence in UV region, as shown in Fig. 2. Two characteristic emissions in the range of 235 – 271 nm were observed. The UC emissions that centered at 244 nm and 256 nm originated from the $^2I_{11/2} \rightarrow {}^4I_{15/2}$ and $^4D_{7/2} \rightarrow {}^4I_{15/2}$ transitions of Er^{3+}, respectively.[42, 43, 48] In Yb^{3+}-Er^{3+} codoped $NaLuF_4$ nanocrystals, the successive energy transfer (ET) from Yb^{3+} ions to Er^{3+} is crucial important for populating the high energy states of Er^{3+}. Figure 3 gives the possible UC population ways in energy level diagrams of Yb^{3+} and Er^{3+} ions.[49, 50] The population processes for the UV ($^2I_{11/2}$ and $^4D_{7/2}$) levels of Er^{3+} can be clearly described as: $^4I_{15/2} \xrightarrow{ET} {}^4I_{11/2} \xrightarrow{ET} {}^4F_{7/2} \xrightarrow{NR} {}^2H_{11/2}$, $^4S_{3/2} \xrightarrow{ET} {}^2G_{7/2} \xrightarrow{NR} {}^4G_{11/2}$,

$^2H_{9/2} \xrightarrow{ET} {}^2D_{5/2} \xrightarrow{NR} {}^2K_{13/2} \xrightarrow{ET} {}^2I_{11/2} \xrightarrow{NR} {}^4D_{7/2}$, where NR represents the nonradiative relaxation from excited Er^{3+} to their lower levels.

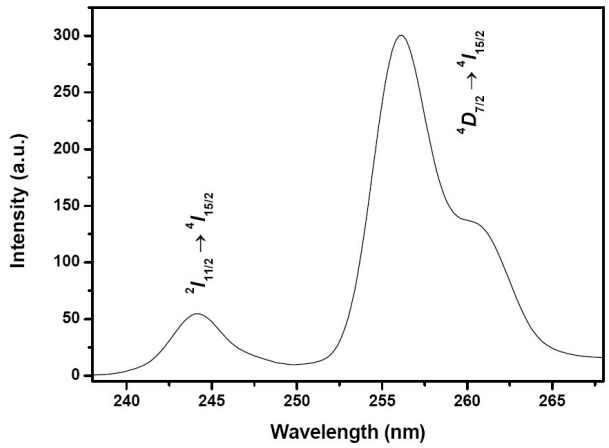

Fig. 2 UC emission spectrum of β-$NaLuF_4$:Yb^{3+}/Er^{3+} nanocrystals in the range of 235 – 271 nm.

To investigate the thermally population behaviors of the $^2I_{11/2}$ and $^4D_{7/2}$ levels of Er^{3+}, the 244 nm and 256 nm UC emissions were discussed by a change of sample temperature from 300 K to 525 K. Figure 4(a) displays the corresponding temperature-dependent UCL spectra of $NaLuF_4$:Yb^{3+}/Er^{3+} nanocrystals. There was nearly no overlap of emission bands from the $^2I_{11/2} \rightarrow {}^4I_{15/2}$ and $^4D_{7/2} \rightarrow {}^4I_{15/2}$ transitions of Er^{3+}, which was benefit for the measuring accuracy of their emission intensities. Additionally, it is obvious that the emission intensities from 244 nm and 256 nm changed greatly with the enhancement of sample temperature. The detailed variation of the integrated emission intensities of I_{244} and I_{256}, as calculated from the UCL spectra, is shown in Fig. 4(b). Obviously, the emission intensity of I_{256} is stronger than that of I_{244} in the whole investigated temperature range. In addition, both the I_{244} and I_{256} decreased with increasing the sample temperature from 300 K to 525 K, which is mainly attributed to the thermal quenching.

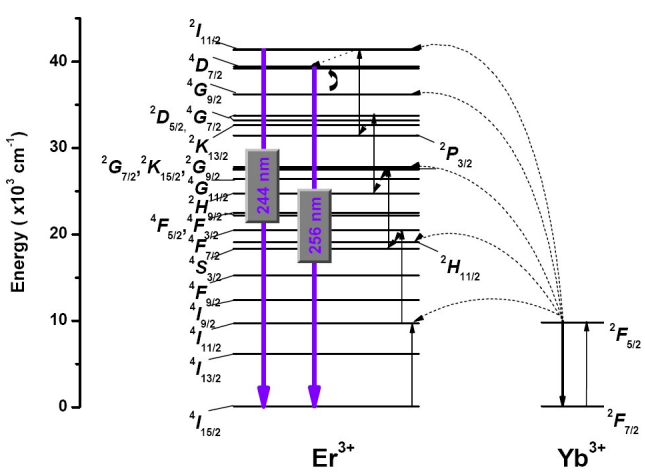

Fig. 3 Energy level diagrams of Yb^{3+} and Er^{3+} ions as well as the proposed UC processes.

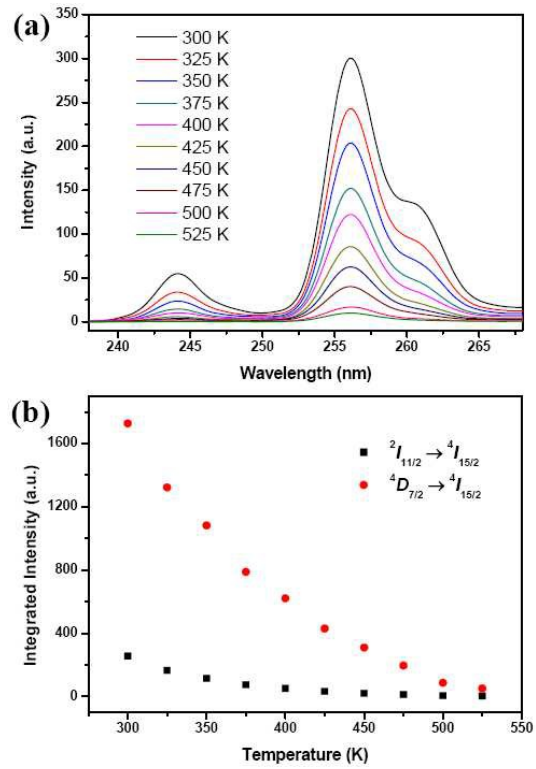

Fig. 4 (a) Temperature-dependent UCL spectra of β-$NaLuF_4$:Yb^{3+}/Er^{3+} nanocrystals in the range of 235 – 271 nm; (b) Temperature-dependent integrated emission intensities of $^2I_{11/2} \rightarrow {}^4I_{15/2}$ and $^4D_{7/2} \rightarrow {}^4I_{15/2}$ transitions of Er^{3+}.

For clarity, all UCL spectra in Fig. 4(a) have been normalized to compare the relative intensity ratio between I_{244} and I_{256}. Figure 5(a) shows the corresponding normalized UCL spectra of the $NaLuF_4$:Yb^{3+}/Er^{3+} nanocrystals from 235 nm to 271 nm. They were measured from 300 K to 525 K, and normalized at 244 nm. It is clear that the relative intensity ratio of I_{244}/I_{256} decreased dramatically with the enhancement of sample temperature. According to Boltzmann distribution, the intensity ratios of I_{upper}/I_{lower} from a pair of thermally coupled levels should increase with increasing the temperature, which is contrary to our experimental results. Therefore, we concluded that the $^2I_{11/2}$ and $^4D_{7/2}$ levels of Er^{3+} are non-thermally coupled levels. To further investigate the temperature-dependent population processes of $^2I_{11/2}$ and $^4D_{7/2}$ levels, we calculated the intensity change ratio of I_{244} ($^2I_{11/2} \rightarrow {}^4I_{15/2}$) and I_{256} ($^4D_{7/2} \rightarrow {}^4I_{15/2}$) of Er^{3+}, as depicted in Fig. 5(b). Here, the intensity change ratio is defined as $(I_0–I)/I_0$, where I_0 and I present the integrated UC emission intensities before and after the temperature changes, respectively. (i.e., I_0 and I are the UC emission intensities recording at 325 K and 350 K, respectively, for the data point at 350 K in Fig 5(b)). As such, it is worthwhile to point out that the intensity change ratios of these two transitions are different. The intensity change ratio of $^2I_{11/2} \rightarrow {}^4I_{15/2}$ transition of Er^{3+} are lager than that of their $^4D_{7/2} \rightarrow {}^4I_{15/2}$ transition in the whole temperature range, as depicted in Fig 5(b), and the corresponding explanation is described below.

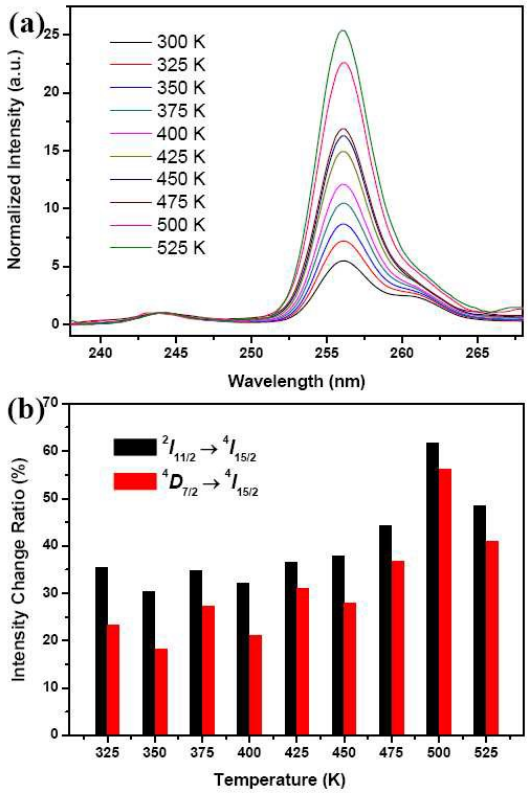

Fig. 5 (a) Temperature-dependent normalized UCL spectra of β-$NaLuF_4$:Yb^{3+}/Er^{3+} nanocrystals. All spectra have been normalized to the emission intensities from the $^2I_{11/2} \rightarrow {}^4I_{15/2}$ transition of Er^{3+}; (b) Temperature dependence of emission intensity change ratios of $^2I_{11/2} \rightarrow {}^4I_{15/2}$ and $^4D_{7/2} \rightarrow {}^4I_{15/2}$ transitions of Er^{3+}.

As shown in Fig 4(b), both the I_{244} and I_{256} decreased with increasing the sample temperature from 300 K to 525 K. However, the change speeds of integrated emission intensities from $^2I_{11/2} \rightarrow {}^4I_{15/2}$ and $^4D_{7/2} \rightarrow {}^4I_{15/2}$ transitions of Er^{3+} are totally different (Fig. 5(b)). From the energy level diagram as displayed in Fig. 3, there is a nonradiative relaxation process from $^2I_{11/2}$ to $^4D_{7/2}$ levels of Er^{3+}, thus, the upconverted population from these two states can be affected by the sample temperature. The higher temperature is the larger multiphonon relaxation rate of $^2I_{11/2} \rightarrow {}^4D_{7/2}$ is. As a result, the UC emissions from $^2I_{11/2} \rightarrow {}^4I_{15/2}$ and $^4D_{7/2} \rightarrow {}^4I_{15/2}$ transitions of Er^{3+} decreased and enhanced, respectively, due to the effective NR process as sample temperature increased from 300 K to 525 K. However, compared with thermal quenching, the NR process of $^2I_{11/2} \rightarrow {}^4D_{7/2}$ played a relatively small effect on the population of $^4D_{7/2}$ level of Er^{3+}. Hence, the total population of $^4D_{7/2}$ state decreased gradually with increasing the sample temperature, as displayed in Fig. 4(b). Furthermore, as reported in our previous work, the $^4D_{7/2}$ state of Er^{3+} was thermally populated from their lower $^4G_{9/2}$ level, leading to the enhanced population of $^4D_{7/2}$ level with the increase of sample temperature as well.[45] To sum up, during the upconverted population processes, the nonradiative relaxation and the thermally population worked simultaneously, resulting in the intensity change ratios of 244 nm ($^2I_{11/2} \rightarrow {}^4I_{15/2}$) UC emissions are larger than those of 256 nm ($^4D_{7/2} \rightarrow {}^4I_{15/2}$). Just because of the different temperature-dependent variation properties of 244 nm and 256 nm UCLs of Er^{3+}, their $^2I_{11/2}$ and $^4D_{7/2}$ levels can be used as thermally-related levels to detect temperature by using FIR method.

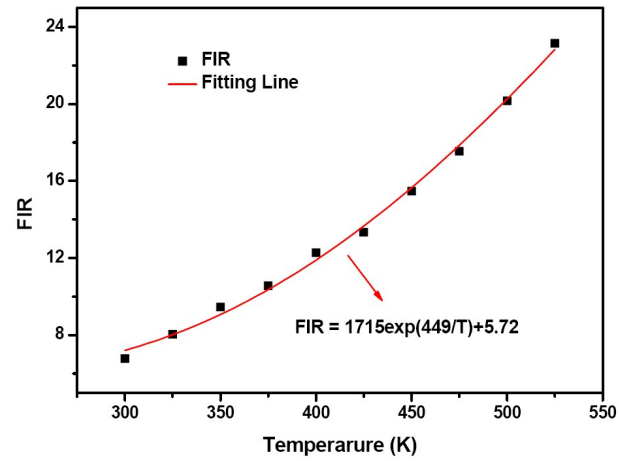

Fig. 6 Temperature dependence of the FIR between the integrated intensities of $^2I_{11/2} \rightarrow {}^4I_{15/2}$ and $^4D_{7/2} \rightarrow {}^4I_{15/2}$ transitions of Er^{3+} in β-$NaLuF_4$:Yb^{3+}/Er^{3+} nanocrystals as well as fitting result.

Figure 6 shows the change of FIR of UV UCLs (I_{256}/I_{244}) of Er^{3+} with increasing the absolute temperature from 300 K to 525 K. By fitting data points according to the equation of $C\exp(-\Delta E/kT)$, the obtained values of C and ΔE were about 1715 and 449 cm^{-1}, respectively. Notably, the slope of the fitting curve increased gradually with the enhancement of sample temperature, as shown in Fig. 6. To further investigate the temperature sensing performance, it is critical for us to discuss the sensor sensitivity S for an optical thermometer. The rate in which FIR varies with absolute temperature, i.e. S, can be defined as: $S = \frac{d[FIR]}{dT} = FIR(\frac{-\Delta E_{12}}{kT^2})$. The corresponding sensitivity curve of this non-thermal coupled levels-based sensor is given in Fig. 7. Obviously, the sensor sensitivity increased dramatically with the enhancement of sample temperature. The value of S reached the maximum of 0.106 K^{-1} at 525 K. A cycle test with high repeatability was obtained in $NaLuF_4$:Yb^{3+}/Er^{3+} nanocrystals. To our knowledge, it is the first time that optical thermometer was obtained by using the non-thermally coupled UV levels of Er^{3+} ions.

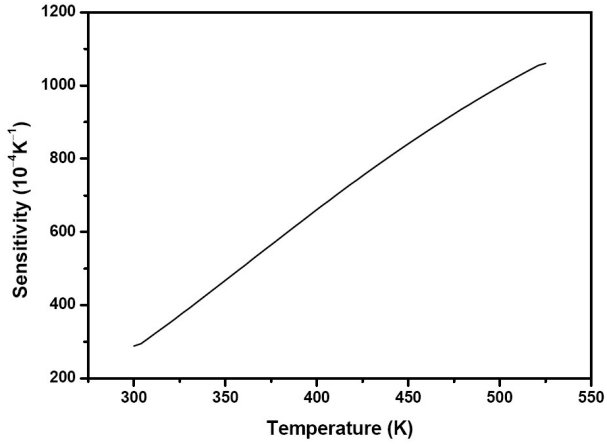

Fig. 7 Sensor sensitivity based on $^2I_{11/2} \rightarrow {}^4I_{15/2}$ and $^4D_{7/2} \rightarrow {}^4I_{15/2}$ transitions of Er^{3+} as a function of the temperature in the range from 300 K to 525 K.

At last, it is critical important to compare the sensitivity of this optical thermometer with those of other RE^{3+}-based temperature sensors. Table 1 lists the sensitivities of several typical temperature sensors based on FIR technique doped with different RE^{3+} ions. It is noteworthy that all the sensor sensitivities are detected by using thermal coupled levels of RE^{3+} except for this work, where the sensitivity is obtained by virtue of the $^2I_{11/2}$ and $^4D_{7/2}$ non-thermally coupled levels of Er^{3+}. From Table 1, we found that the sensitivity achieved in this work is the highest among all sensors. Therefore, we concluded that the use of non-thermally coupled levels of Er^{3+} is an effective approach to enhance the sensor sensitivity of optical thermometers.

Ions (host)	Transitions	S_{max} ($10^{-4}K^{-1}$)	Temperature Range (K)	Reference
Gd (β–$NaLuF_4$)	$^6P_{5/2}$, $^6P_{7/2} \rightarrow {}^8S_{7/2}$	4.05	298 – 523	14
Er (fluorotellurite glass)	$^2H_{11/2}$, $^4S_{3/2} \rightarrow {}^4I_{15/2}$	54	300 – 550	19
Er-Mo ($Yb_3Al_5O_{12}$)	$^2H_{11/2}$, $^4S_{3/2} \rightarrow {}^4I_{15/2}$	48	295 – 973	36
Er ($LiNbO_3$)	$^2H_{11/2}$, $^4S_{3/2} \rightarrow {}^4I_{15/2}$	121	285 – 453	35
Er ($CaWO_4$)	$^4G_{11/2}$, $^2H_{9/2} \rightarrow {}^4I_{15/2}$	190	300 – 873	40
Nd (glass ceramic)	$^4F_{5/2}$, $^4F_{3/2} \rightarrow {}^4I_{9/2}$	15	300 – 700	48
Nd (β–$NaYF_4$)	$^4F_{5/2}$, $^4F_{3/2} \rightarrow {}^4I_{9/2}$	280	323 – 673	42
Ho (Y_2O_3)	$^3K_8$, $^5F_3 \rightarrow {}^5I_8$	30.2	299 – 673	49
Ho (β–$NaLuF_4$)	$^5F_1/^5G_6$, $^5F_{2,3}/^3K_8 \rightarrow {}^5I_8$	14	390 – 780	50
Ho (glass ceramic)	$^5F_1/^5G_6$, $^5F_{2,3}/^3K_8 \rightarrow {}^5I_8$	1.21	303 – 643	51
Tm ($LiNbO_3$)	$^3F_{2,3}$, $^3H_4 \rightarrow {}^3H_6$	0.12	323 – 733	52
Dy ($Y_4Al_2O_9$)	$^4I_{15/2}$, $^4F_{9/2} \rightarrow {}^6H_{15/2}$	30	296 – 973	53
Pr ($NaYF_4$)	$^3P_0$, $^3P_1 \rightarrow {}^3H_5$	135.2	100 – 300	54
Er (β–$NaLuF_4$)	$^2I_{11/2}$, $^4D_{7/2} \rightarrow {}^4I_{15/2}$	1060	300 – 525	this work

Table 1 Sensitivities of optical temperature sensors based on the fluorescence of materials with RE^{3+} as activators.

Conclusions

In conclusion, a strategy for enhancing the sensitivity of optical temperature sensor is put forward here by using the FIR between non-thermal coupled levels of Er^{3+}. Under 980 nm laser excitation, UV UCLs from the $^2I_{11/2} \rightarrow {}^4I_{15/2}$ (244 nm) and $^4D_{7/2} \rightarrow {}^4I_{15/2}$ (256 nm) transitions of Er^{3+} ions were observed in Yb^{3+}-Er^{3+} codoped β-$NaLuF_4$ nanocrystals. By investigating their different thermal population behaviors, optical temperature sensing performance based on the non-thermal coupled levels of $^2I_{11/2}$ and $^4D_{7/2}$ was fulfilled in this work for the first time. The obtained maximum sensor sensitivity is 0.106 K^{-1} at 525 K, which is prior to those of other RE^{3+}-based optical thermometer by using thermal coupled levels-based FIR technique. This excellent temperature sensing performance based on the UV UCLs of Er^{3+}, combined with their imaging characteristics, made Er^{3+}-based UCL materials potential candidates for multifunctional biomedical applications.

Acknowledgments

This work was supported by the National Natural Science Foundation of China (NNSFC) (grants 11404136, 11474132, and 11274139), China Postdoctoral Science Foundation (2012M520668), and Scientific and Technological Developing Project of Jilin Province (20150520028JH).

Notes and references

State Key Laboratory on Integrated Optoelectronics, College of Electronic Science and Engineering, Jilin University, Changchun 130012, China. Fax: +86-431-85168241-8325; Tel: +86-431-85153853; E-mail: wpqin@jlu.edu.cn.

1 L. H. Fischer, G. S. Harms, and O. S. Wolfbeis, *Angew. Chem. Int. Ed.*, 2011, **50**, 4546.
2 T. B. Huff, L. Tong, Y. Zhao, M. N. Hansen, J.X. Cheng, and A. Wei, *Nanomedicine*, 2007, **2**, 125.
3 D. Jaque, F. Vetrone, *Nanoscale* 2012, **4**, 4301.
4 P. R. N. Childs, J. R. Greenwood, and C. A. Long, *Rev. Sci. Instrum.*, 2000, **71**, 2959.
5 C. D. S. Brites, P. P. Lima, N. J. O. Silva, A. Millán, V. S. Amaral, F. Palacio, and L. D. Carlos, *Adv. Mater.*, 2010, **22**, 4499.
6 G. W. Walker, V. C. Sundar, C. M. Rudzinski, A. W. Wun, M. G. Bawendi, and D. G. Nocera, *Appl. Phys. Lett.*, 2003, **83**, 3555.
7 S. Ebert, K. Travis, B. Lincoln, and J. Guck, *Opt. Express*, 2007, **15**, 15493.
8 D. Ross, M. Gaitan, and L. E. Locascio, *Anal. Chem.*, 2001, **73**, 4117.
9 V. A. Vlaskin, N. Janssen, J. van Rijssel, R. Beaulac, and D. R. Gamelin, *Nano Lett.*, 2010, **10**, 3670.

10 Y. Cui, H. Xu, Y. Yue, Z. Guo, J. Yu, Z. Chen, J. Gao, Y. Yang, G. Qian, and B. Chen, *J. Am. Chem. Soc.*, 2012, **134**, 3979.
11 P. V. dos Santos, M. T. de Araujo, A. S. Gouveia-Neto, J. A. Medeiros Neto, and A. S. B. Sombra, *Appl. Phys. Lett.*, 1998, **73**, 578.
12 M. T. Carlson, A. J. Green, and H. H. Richardson, *Nano Lett.*, 2012, **12**, 1534.
13 S. H. Zheng, W. B. Chen, D. Z. Tan, J. J. Zhou, Q. B. Guo, W. Jiang, C. Xu, X. F. Liu, and J. R. Qiu, *Nanoscale*, 2014, **6,** 5675.
14 K. Z. Zheng, Z. Y. Liu, C. J. Lv, and W. P. Qin, *J. Mater. Chem. C*, 2013, **1,** 5502.
15 Y. H. Han, C. B. Tian, Q. H. Li, and S. W. Du, *J. Mater. Chem. C*, 2014, **2,** 8065.
16 Carlos D. S. Brites, Patricia P. Lima, Nuno J. O. Silva, Angel Millán, Vitor S. Amaral, Fernando Palacio, and Luís D. Carlos, *New J. Chem.*, 2011, **35**, 1177.
17 Andreas Sedlmeier, Daniela E. Achatz, Lorenz H. Fischer, Hans H. Gorris, and Otto S. Wolfbeis, *Nanoscale* 2012, **40**, 7090.
18 Márcio A. R. C. Alencar, Glauco S. Maciel, and Cid B. de Araújo, *Appl. Phys. Lett.*, 2004, **84**, 4753.
19 S. F. León-Luis, U. R. Rodríguez-Mendoza, E. Lalla, and V. Lavín, *Sensors and Actuators B*, 2011, **158,** 208.
20 R. K. Verma, S. B. Rai, *J. Quant. Spectrosc. Ra.*, 2012, **113,** 1594.
21 D. Wawrzynczyk, A. Bednarkiewicz, M. Nyk, W. Strek, and M. Samoc, *Nanoscale*, 2012, **4,** 6959.
22 F. Vetrone, R. Naccache, A. Zamarron, A. J. de la Fuente, F. Sanz-Rodriguez, L. M. Maestro, E. M. Rodriguez, D. Jaque, J. G. Sole, and J. A. Capobianco, *ACS Nano*, 2010, **4,** 3254.
23 F. Auzel, *Chem. Rev*., 2004, **104**, 139.
24 Y. Liu, D. Tu, H. Zhu, R. Li, W. Luo, and X. Chen, *Adv. Mater*., 2010, **22**, 3266.
25 L. Lei, D. Chen, P. Huang, J. Xu, R. Zhang, and Y. Wang, *Nanoscale*, 2013, **5**, 11298.
26 D. J. Gargas, E. M. Chan, A. D. Ostrowski, S. Aloni, M. V. P. Altoe, E. S. Barnard, B. Sanii, J. J. Urban, and D. J. Milliron, *Nat. Nanotechnology*, 2014, **9**, 300.
27 L. Zhou, R. Wang, C. Yao, X. M. Li, C. L. Wang, X. Y. Zhang, C. J. Xu, A. J. Zeng, D. Y. Zhao, and F. Zhang, *Nat. Comm.*, 2015, **6**, 6938, doi:10.1038/ncomms7938.
28 R. R. Deng, F. Qin, R. F. Chen, W. Huang, M. H. Hong, and X. G. Liu, *Nat. Nanotechnology*, 2015, **10**, 237.
29 Y. Liu, M. Chen, T. Cao, Y. Sun, C. Li, Q. Liu, T. Yang, L. Yao, W. Feng, and F. Li, *J. Am. Chem. Soc.*, 2013**, 135**, 9869.
30 Q. Chen, C. Wang, L. Cheng, W. W. He, Z. P. Cheng, and Z.Liu, *Small*, 2014**, 10**, 1544.
31 Z. Y. Hou, Y. X. Zhang, K. R. Deng, Y. Y. Chen, X. J. Li, X. R. Deng, Z. Y. Cheng, H. Z. Lian, C. X. Li, and J. Lin, *ACS Nano*, 2015, **9**, 2584.
32 X. Teng, Y. H. Zhu, W. Wei, S. C. Wang, J. F. Huang, R. Naccache, W. B. Hu, A. I. Y Tok, Y. Han, Q. C. Zhang, Q. L. Fan, W. Huang, J. A. Capobianco, and L. Huang, *J. Am. Chem. Soc*, 2012, **134,** 8340.
33 D. Wang, B. Xue, X. G. Kong, L. P. Tu, X. M. Liu, Y. L. Zhang, Y. L. Chang, Y. S. Luo, H. Y. Zhao, and H. Zhang, *Nanoscale*, 2015, **7,** 190.
34 J. B. Zhao, D. Y. Jin, E. P. Schartner, Y. Q. Lu, Y. J. Liu, A. V. Zvyagin, L. X. Zhang, J. M. Dawes, P. Xi, J. A. Piper, E. M. Goldys, T. M. Monro, *Nat. Nanotechnology*, 2013, **8**, 729.
35 H. Dong, L. D. Sun, Y. F. Wang, J. Ke, R. Si, J. W. Xiao, G. M. Lyu, S. Shi, and C. H. Yan, *J. Am. Chem. Soc*, 2015, **137,** 6569.
36 S. Zeng, Z. Yi, W. Lu, C. Qian, H. Wang, L. Rao, T. Zeng, H. Liu, H. Liu, B. Fei, and J. Hao, *Adv. Funct. Mater*., 2014, **24**, 4051.
37 S. Zeng, H. Wang, W. Lu, Z. Yi, L. Rao, H. Liu, and J. Hao, *Biomaterials*, 2014, **35**, 2934.
38 Z. Yi, W. Lu, H. Liu, and S. Zeng, *Nanoscale*, 2015, **7**, 542.
39 M. Quintanilla, E. Cantelar, F. Cussó, M. Villegas, and A. C. Caballero, *Appl. Phys. Express*, 2011, **4,** 022601.
40 B. Dong, B. S. Cao, Y. Y. He, Z. Liu, Z. P. Li, and Z. Q. Feng, *Adv. Mater*., 2012, **24,** 1987.
41 N. Rakov, G. S. Maciel, *Sensors and Actuators B*, 2012, **164,** 96.
42 K. Z. Zheng, D. Zhao, D. S. Zhang, N. Liu, and W. P. Qin, *J. Fluo. Chem.*, 2011, **132,** 5.
43 K. Z. Zheng, D. Zhao, D. S. Zhang, N. Liu, and W. P. Qin, *Opt. Lett.*, 2010, **35,** 2442.
44 W. Xu, Z. G. Zhang, and W. W. Cao, *Opt. Lett.*, 2012, **37,** 4865.
45 K. Z. Zheng, W. Y. Song, G. H. He, Z. Yuan, and W. P. Qin, *Opt. Express*, 2015, **23**, 7653.
46 X. N. Tian, X. T. Wei, Y. H. Chen, C. K. Duan, and M. Yin, *Opt. Express*, 2014, **22**, 30333.
47 F. Shi, J. S. Wang, X. S. Zhai, D. Zhao, and W. P. Qin, *CrystEngComm.*, 2011, **13,** 3782.
48 G. Y. Chen, H. Liang, H. Liu, G. Somesfalean, and Z. G. Zhang, *Opt. Express*, 2009, **17,** 16366.
49 W.T. Carnall, P.R. Fields, and K. Rajnak, *J. Chem. Phys.*, 1968, **49**, 4412.
50 W.T. Carnall, P.R. Fields, and K. Rajnak, *J. Chem. Phys.*, 1968, **49**, 4424.
51 P. Haro-Gonzalez, I. R. Martin, L. L. Martin, S. F. Leon-Luis, C. Perez-Rodriguez, V. Lavin, *Opt. Mater.*, 2011, **33,** 742.
52 A. Pandey, V. K. Rai, *Dalton T.*, 2013, **42,** 11005.
53 S. S. Zhou, S. Jiang, X. T. Wei, Y. H. Chen, C. K. Duan, and M. Yin, *J. Alloys Comp.*, 2014, **588,** 654.
54 W. Xu, X. Y. Gao, L. J. Zheng, Z. G. Zhang, and W. W. Cao, *Opt. Express*, 2012, **20,** 18127.
55 L. L. Xing, Y. L. Xu, R. Wang, W. Xu, and Z. G. Zhang, *Opt. Lett.*, 2014, **39,** 454.
56 Z. Boruc, M. Kaczkan, B. Fetlinski, S. Turczynski, M. Malinowski, *Opt. Lett.*, 2012, **37,** 5214.
57 S. S. Zhou, G. C. Jiang, X. T. Wei, C. K. Duan, Y. H. Chen, and M. Yin, *J. Nanosci. Nanotechno.*, 2014, **14,** 3739.